Eur. Phys. J. B (2014) 87: 184
DOI: 10.1140/epjb/e2014-50267-1

THE EUROPEAN PHYSICAL JOURNAL B

Regular Article

On stochastic spatial patterns and neuronal polarity

Silvia A. Menchón[1,a] and Horacio S. Wio[2]

[1] IFEG-CONICET & FaMAF-UNC, Medina Allende s/n, 5000 Córdoba, Argentina
[2] IFCA (UC-CSIC), Avda. de los Castros s/n, 39005 Santander, Spain

Received 24 April 2014 / Received in final form 18 June 2014
Published online 7 August 2014 –

Abstract. Polarization refers to asymmetric changes in cellular organization that occur in response to external or internal signals. Although neurons can spontaneously establish and maintain asymmetric distributions of signaling molecules on the plasma membrane, it is not clear how intrinsic noise affects neuronal polarization. In this work we present a stochastic model based on endocytosis, exocytosis and lateral diffusion, to study the effects of low number of molecules (high noise intensity), on neuronal polarization. Numerical results were obtained by solving the master equation using Gillespie's algorithm. Our model suggests that the formation of a single pole of molecular asymmetry is very robust to noise; furthermore, in the presence of noise, neuronal polarization could occur even with reduced feedback strength.

1 Introduction

During the first stage of neuronal polarity a symmetry breaking event takes place [1]. Before the first neurite starts growing, some membrane proteins and members of the Rho GTPases family show spatially localized distributions on the cell membrane [2]. These asymmetric distributions are established spontaneously and can be maintained even without the action of external cues. Some mechanisms, such as positive feedbacks, are thought to be central to the process of polarized domain formation. Although neuronal polarity also occurs in very controlled environments, as it is the case of in vitro experiments, it is impossible to avoid intrinsic noise.

Several mathematical models have shown the importance of positive feedback loops in cell polarity. In particular, some of them state that feedback alone can spontaneously establish a single site of polarity [3,4]. However, it is also suggested that polarization could be very sensitive to stochastic fluctuations. One of the issues giving rise to controversy is the relationship between the amount of involved particles and polarization. Altschuler et al. presented a stochastic model where cells could polarized only when the number of molecules is small [3]. Although using the same model, Grupta showed that it is possible to obtain cell polarity in the infinite population limit, if the feedback strength increases linearly with the population size [5]. Walther et al. determined a threshold number of molecules required for robust polarization [6] and Freisinger and co-workers found that polarity establishment does not depend on the quantity of molecules [7].

In this work we present a model to analyze how intrinsic noise affects neuronal polarity. As intrinsic noise is scaled with the system size, our model allows us to analyze how molecule number fluctuations affect cell polarity in systems with a finite number of molecules. The model itself is the stochastic version of that presented in reference [8]. This model considers the interaction between membrane proteins and modulators of endocytosis (for instance, members of the Rho GTPases family). In order to formulate the stochastic version, we write down a master equation considering the reactions between molecules. Its linear noise approximation is derived using van Kampen's system size expansion [9,10]. Our approach indicates that Turing patterns are not spoiled by intrinsic noise and quasi-pattern structures can be formed with less positive feedback intensity. Since in this approach more noise intensity is associated to a small number of particles, we found that Turing pattern formation does not depend on the number of molecules, but quasi-patterns are not well established if the amount of molecules is too large or too small. Our model suggests that neuronal polarity is very robust to noise, furthermore, in the presence of noise it could occur even with reduced feedback strength.

2 The model

We formulate our model considering two different kinds of molecules, one that represents a typical integral membrane protein endocytosed by a canonical clathrin-mediated process (e.g., cadherin); and another one, representing a modulator of endocytosis (e.g., p. 120-catenin or Rho GTPases). As described in reference [8], we consider the following biological events:

1. *Spontaneous membrane association:* Membrane proteins are tethered spontaneously to the cell membrane [11,12].

[a] e-mail: menchon@famaf.unc.edu.ar

2. *Membrane association through recruitment:* A positive feedback circuit recruits membrane proteins to the places where they are already localized [3,13].
3. *Endocytosis:* Endocytosis pathway is regulated by the amount of modulators of endocytosis [14,15].
4. *Spontaneous activation:* Modulators of endocytosis are activated spontaneously [16].
5. *Deactivation:* Modulators of endocytosis are deactivated [16].
6. *Activation through recruitment:* The activation of modulators of endocytosis is also induced by membrane proteins [17].
7. *Lateral diffusion:* Membrane proteins and modulators of endocytosis diffuse on the cell membrane.

We assume that membrane proteins, A, and modulator of endocytosis, B, inhabit patches labeled by $i = 1, \ldots, \Omega$, each of which has volume V. The number of A and B molecules at patch i are denoted by n_i and m_i, respectively. Taking into account the biological events we described above, the reactions/interactions between A and B molecules at each patch are represented by:

$$\begin{aligned} \emptyset_i &\xrightarrow{k_1} A_i, \\ A_i &\xrightarrow{r_1 k_1} 2A_i, \\ A_i + B_i &\xrightarrow{k_2 h(n_i/V)} B_i, \\ \emptyset_i &\xrightarrow{k_3} B_i, \\ A_i &\xrightarrow{r_3 k_3} A_i + B_i, \\ B_i &\xrightarrow{k_4} \emptyset_i, \end{aligned} \tag{1}$$

where the symbol $\emptyset$ means "empty" and the index i runs from 1 to Ω. The rate for each reaction is indicated above its arrow; A_i and B_i denote molecules in patch i at the time the reaction occurs. We consider that the reaction $A_i + B_i \xrightarrow{k_2 h(n_i/V)} B_i$ has a non constant rate. In particular, we adopt $h(x) = 1/(1 + r_2 x)$, that is equivalent to consider a Michaelis-Menten kinetics in the macroscopic equations [18].

In addition, we also consider migration reactions, which describe molecular diffusion from one patch to another. In this work we consider the cell membrane as a one dimensional regular lattice with periodic boundary conditions and homogeneous diffusion coefficients. Then, molecules in patch i can diffuse in or out of a neighboring patch j through the following reactions:

$$\begin{aligned} A_i &\xrightarrow{\delta_1} A_j, \qquad A_j \xrightarrow{\delta_1} A_i, \\ B_i &\xrightarrow{\delta_2} B_j, \qquad B_j \xrightarrow{\delta_2} B_i. \end{aligned} \tag{2}$$

Let $T(\mathbf{n}', \mathbf{m}'|\mathbf{n}, \mathbf{m})$ be the transition rate from the state $(\mathbf{n}, \mathbf{m})$ to the state $(\mathbf{n}', \mathbf{m}')$, where $\mathbf{n}$ and $\mathbf{m}$ are vectors whose components are n_i and m_i, respectively. Assuming a perfect mixing in each individual patch, the local and migration transition rates are:

$$\begin{aligned} T(n_i + 1, m_i|n_i, m_i) &= \left(k_1 + r_1 k_1 \frac{n_i}{V}\right) \frac{1}{\Omega}, \\ T(n_i - 1, m_i|n_i, m_i) &= k_2 h(n_i/V) \frac{n_i}{V} \frac{m_i}{V} \frac{1}{\Omega}, \\ T(n_i, m_i + 1|n_i, m_i) &= \left(k_3 + r_3 k_3 \frac{n_i}{V}\right) \frac{1}{\Omega}, \\ T(n_i, m_i - 1|n_i, m_i) &= k_4 \frac{m_i}{V} \frac{1}{\Omega}, \\ T(n_i - 1, n_j + 1|n_i, n_j) &= \delta_1 \frac{n_i}{V} \frac{1}{2\Omega}, \\ T(n_i + 1, n_j - 1|n_i, n_j) &= \delta_1 \frac{n_j}{V} \frac{1}{2\Omega}, \\ T(m_i - 1, m_j + 1|m_i, m_j) &= \delta_2 \frac{m_i}{V} \frac{1}{2\Omega}, \\ T(m_i + 1, m_j - 1|m_i, m_j) &= \delta_2 \frac{m_j}{V} \frac{1}{2\Omega}. \end{aligned} \tag{3}$$

In order to write down these expressions, we consider, for instance, that the probability of picking A_i and B_i is proportional to $(n_i/V)(m_i/V)/\Omega$. The migration terms correspond to diffusion in a one dimensional grid of Ω nodes. For a detailed explanation of how to obtain the transitions rates, we suggest to see references [19–24].

Assuming the process defined by equations (3) as a one-step Markov process, we can write down a master equation given by:

$$\begin{aligned} \frac{\partial P(\mathbf{n}, \mathbf{m}, t)}{\partial t} &= \sum_{i=1}^{\Omega} \mathcal{T}_i^{loc} P(\mathbf{n}, \mathbf{m}, t) \\ &\quad + \sum_{i=1}^{\Omega} \sum_{j \leftrightarrow i} \mathcal{T}_{ij}^{mig} P(\mathbf{n}, \mathbf{m}, t), \end{aligned} \tag{4}$$

where the sum over $j \leftrightarrow i$ indicates that j is a nearest neighbor of i and the operators $\mathcal{T}_i^{loc}$ and $\mathcal{T}_{ij}^{mig}$ contain the local and migration transition rates, respectively. Defining the operators $\mathbb{E}_{n_i}^{\pm 1}$ and $\mathbb{E}_{m_i}^{\pm 1}$ as follows [9,10]

$$\begin{aligned} &\mathbb{E}_{n_i}^{\pm 1} f(n_1, \ldots, n_i, \ldots, n_\Omega, \mathbf{m}) \\ &\qquad = f(n_1, \ldots, n_i \pm 1, \ldots, n_\Omega, \mathbf{m}), \\ &\mathbb{E}_{m_i}^{\pm 1} f(\mathbf{n}, m_1, \ldots, m_i, \ldots, m_\Omega) \\ &\qquad = f(\mathbf{n}, m_1, \ldots, m_i \pm 1, \ldots, m_\Omega), \end{aligned}$$

and doing the transformation $t \to t/(V\Omega)$, yields:

$$\begin{aligned} \mathcal{T}_i^{loc} &= \left(\mathbb{E}_{n_i}^{-1} - 1\right)(V k_1 + r_1 k_1 n_i) \\ &\quad + (\mathbb{E}_{n_i} - 1) k_2 h(n_i/V) n_i m_i / V \\ &\quad + \left(\mathbb{E}_{m_i}^{-1} - 1\right)(V k_3 + r_3 k_3 n_i) + (\mathbb{E}_{m_i} - 1) k_4 m_i, \\ \mathcal{T}_{ij}^{mig} &= \left(\mathbb{E}_{n_i} \mathbb{E}_{n_j}^{-1} - 1\right) \delta_1 n_i / z + \left(\mathbb{E}_{n_j} \mathbb{E}_{n_i}^{-1} - 1\right) \delta_1 n_j / z \\ &\quad + \left(\mathbb{E}_{m_i} \mathbb{E}_{m_j}^{-1} - 1\right) \delta_2 m_i / z + \left(\mathbb{E}_{m_j} \mathbb{E}_{m_i}^{-1} - 1\right) \delta_2 m_j / z. \end{aligned} \tag{5}$$

The master equation contains information of both the mean-field dynamics and the finite V corrections. They

$$A_k = \begin{pmatrix} F_\phi(\phi^s,\psi^s) + 2\delta_1(\cos(\ell k)-1) & F_\psi(\phi^s,\psi^s) \\ G_\phi(\phi^s,\psi^s) & G_\psi(\phi^s,\psi^s) + 2\delta_2(\cos(\ell k)-1) \end{pmatrix} \tag{11}$$

can be analyzed by doing a system-size expansion and studying it in the limit of large but finite V [9]. In order to carry out this expansion we apply the transformations $n_i = V\phi_i + V^{1/2}\xi_i$ and $m_i = V\psi_i + V^{1/2}\eta_i$, where ξ_i and η_i stand for the stochastic contributions. The leading order in the perturbative analysis of the master equation in powers of $V^{1/2}$ gives the deterministic equations, while the fluctuations are characterized by the next order. In the next sections we analyze the mean-field solution and the fluctuations. The details of the calculation to obtain the mean-field approximation and the Fokker-Planck equation are given in the Appendix.

3 Mean-field approximation

The mean-field approximation is given by the following macroscopic equations:

$$\frac{d\phi_i}{dt} = k_1(1+r_1\phi_i) - k_2\frac{\phi_i\psi_i}{1+r_2\phi_i} + \delta_1\Delta\phi_i,$$
$$\frac{d\psi_i}{dt} = k_3(1+r_3\phi_i) - k_4\psi_i + \delta_2\Delta\psi_i, \tag{6}$$

where $i = 1,\ldots,\Omega$, and Δ is the discrete Laplacian operator in one dimension:

$$\Delta f_i = \sum_{j\leftrightarrow i}(f_j - f_i). \tag{7}$$

These equations are obtained by doing the system size expansion and taking the terms proportional to $V^{1/2}$ (see the Appendix). The first of equations (6) describes the temporal evolution of ϕ_i. On the right-hand side, the first term has contributions due to spontaneous membrane association and positive feedback, while the second term describes endocytosis with a Michaelis-Menten kinetics; and the last term corresponds to migration. The second of equations (6) describes the temporal evolution of ψ_i. On the right-hand side, the first term represents spontaneous activation and activation through recruitment; the second one represents inhibitor deactivation; and the last one corresponds to migration.

The case $\Omega = 1$ is equivalent to consider the system without diffusion and the limit $\Omega \to \infty$ when the lattice spacing, ℓ, goes to zero corresponds to a continuous description, where equation (6) becomes:

$$\frac{\partial\phi}{\partial t} = k_1(1+r_1\phi) - k_2\frac{\phi\psi}{1+r_2\phi} + \delta_1\nabla^2\phi,$$
$$\frac{\partial\psi}{\partial t} = k_3(1+r_3\phi) - k_4\psi + \delta_2\nabla^2\psi, \tag{8}$$

with the rescaling $\delta_1 \to \delta_1\ell^2$ and $\delta_2 \to \delta_2\ell^2$.

The homogeneous fixed points, (ϕ^s,ψ^s) are given by solving the equations

$$F(\phi^s,\psi^s) \equiv k_1(1+r_1\phi^s) - k_2\frac{\phi^s\psi^s}{1+r_2\phi^s} = 0, \tag{9}$$
$$G(\phi^s,\psi^s) \equiv k_3(1+r_3\phi^s) - k_4\psi^s = 0. \tag{10}$$

If $k_2k_3r_3 < k_4k_1r_1r_2$, or if $k_2k_3r_3 = k_4k_1r_1r_2$ and $k_2k_3 > (r_1+r_2)k_1k_4$, there is only one positive solution, but if $k_2k_3r_3 > k_4k_1r_1r_2$ and $k_2k_3 > (r_1+r_2)k_1k_4$, there are two positive solutions. However, in all these cases only one positive solution is stable (see Ref. [8]). Stability under homogeneous perturbations is guaranteed if $F_\phi(\phi^s,\psi^s) + G_\psi(\phi^s,\psi^s) < 0$ and $F_\phi(\phi^s,\psi^s)G_\psi(\phi^s,\psi^s) - F_\psi(\phi^s,\psi^s)G_\phi(\phi^s,\psi^s) > 0$, where the subindex indicates partial derivative. In order to analyze diffusive instabilities, we include the spatial contributions. Considering the solution $(\phi_j-\phi^s,\psi_j-\psi^s)^T \propto \exp(\lambda t + i\ell kj)$, and defining the matrix

see equation (11) *above*,

it is possible to show that diffusion instabilities are present if at least one of the eigenvalues of A_k has a positive real part for some $k = 2n\pi/L$ with $n \in \mathbb{Z}$. In the limit $\Omega \to \infty$, the lattice space goes to zero and $2(\cos(k\ell)-1) \to -(k\ell)^2$. In this case the conditions for Turing pattern formation are the same than those found in reference [8] (considering the rescaling $\delta_1 \to \delta_1\ell^2$ and $\delta_2 \to \delta_2\ell^2$).

The phase diagram for Turing instability is shown in Figure 1a. Although we used the same notation, the parameters used in reference [8] are not the transition rates that characterize the reactions, but the reaction rate constants. For a more clear comparison with reference [8], we express the numerical values of the reaction rate constants. In order to avoid misunderstanding, we denote the reaction rate constants with the symbol " $\widehat{\cdot}$ ". The diagram in Figure 1a is displayed in the $(\widehat{r}_2,\widehat{r}_1)$ plane, all the other parameters are assumed fixed and they were set as used in reference [8]. The black area indicates the values of $\widehat{r}_1$ and $\widehat{r}_2$ that can generate patterns while all the other kinetic and diffusion parameters are fixed. The system presented here is known as an activator-inhibitor system; which shows Turing instabilities if the inhibitor diffuses faster than the activator [25]. Since membrane proteins are bigger than modulators of endocytosis, the diffusion coefficient of modulators of endocytosis is greater than the diffusion coefficient of membrane proteins [26–28].

4 Intrinsic noise and fluctuations

Considering the terms proportional to V^0 in the system size expansion (see Appendix), we obtain the

$$\left\langle |\xi_k(\omega)|^2 \right\rangle = \frac{\mathcal{B}_{k,11}\left(\omega^2 + \left(G_\psi\left(\phi^s,\psi^s\right) + 2\delta_2(\cos(k\ell)-1)\right)^2\right) + \left(F_\psi\left(\phi^s,\psi^s\right)\right)^2 \mathcal{B}_{k,22}}{\left(\det(A_k)-\omega^2\right)^2 + \omega^2\left(\mathrm{Tr}(A_k)\right)^2} \tag{18}$$

$$\left\langle |\eta_k(\omega)|^2 \right\rangle = \frac{\mathcal{B}_{k,22}\left(\omega^2 + \left(F_\phi\left(\phi^s,\psi^s\right) + 2\delta_1(\cos(k\ell)-1)\right)^2\right) + \left(G_\phi\left(\phi^s,\psi^s\right)\right)^2 \mathcal{B}_{k,11}}{\left(\det(A_k)-\omega^2\right)^2 + \omega^2\left(\mathrm{Tr}(A_k)\right)^2} \tag{19}$$

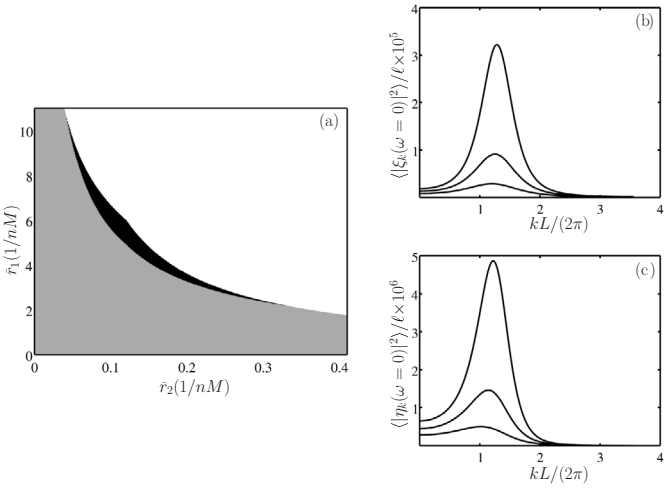

Fig. 1. Phase diagram (a), the black zone stands for Turing pattern formation, i.e. for the parameters in the black zone at least one of the eigenvalues of A_k has a positive real part. In the black and gray zones, power spectra have a maximum. The gray region corresponds to quasi-patterns. The kinetic and diffusion parameters were selected as used in reference [8], $\widehat{k}_1 = 0.025$ nM s^{-1}, $\widehat{k}_2 = 0.003$ nM^{-1} s^{-1}, $\widehat{k}_3 = 2.25$ nM s^{-1}, $\widehat{k}_4 = 0.15$ s^{-1}, $\widehat{r}_3 = 0.4$ nM^{-1}, $\widehat{\delta}_1 = 0.03$ μm^2/s, $\widehat{\delta}_2 = 0.13$ μm^2/s. Power spectra $\langle|\xi_k(\omega=0)|^2\rangle$, (b) and $\langle|\eta_k(\omega=0)|^2\rangle$, (c), for $(\widehat{r}_2, \widehat{r}_1)$ pairs in the gray region. From top to bottom $\widehat{r}_1$ takes the values 3.75 nM^{-1}, 3.65 nM^{-1} and 3.5 nM^{-1}; $\widehat{r}_2 = 0.16$ nM^{-1}.

Fokker-Planck equation:

$$\frac{\partial \Pi}{\partial t} = -\sum_{i=1}^{\Omega} \frac{\partial}{\partial \boldsymbol{\zeta}_i}\left(\mathcal{A}_i\left(\boldsymbol{\zeta}_i\right)\Pi\right) + \frac{1}{2}\sum_{i,j}\frac{\partial^2}{\partial \boldsymbol{\zeta}_i \partial \boldsymbol{\zeta}_j}\left(\mathcal{B}_{i,j}\Pi\right), \tag{12}$$

where $\boldsymbol{\zeta}_i = (\xi_i, \eta_i)$. The functions $\mathcal{A}_i\left(\boldsymbol{\zeta}_i\right)$ and the matrices $\mathcal{B}_{i,j}$ are given by:

$$\begin{aligned}
\mathcal{A}_{i,1} &= \left(r_1 k_1 - k_2 h'(\phi_i)\psi_i\phi_i - k_2 h(\phi_i)\psi_i + \delta_1 \Delta\right)\xi_i \\
&\quad - k_2 h(\phi_i)\phi_i \eta_i, \\
\mathcal{A}_{i,2} &= r_3 k_3 \xi_i + \left(-k_4 + \delta_2 \Delta\right)\eta_i, \\
\mathcal{B}_{ij,11} &= \left(k_1 + r_1 k_1 \phi^s + k_2 h\left(\phi^s\right)\phi^s\psi^s + 4\delta_1\phi^s\right)\delta_{i,j} \\
&\quad - \frac{4\delta_1}{z}\phi^s J_{\langle ij\rangle}, \\
\mathcal{B}_{ij,22} &= \left(k_3 + r_3 k_3 \phi^s + k_4\psi^s + 4\delta_2\psi^s\right)\delta_{i,j} - \frac{4\delta_2}{z}\psi^s J_{\langle ij\rangle}, \\
\mathcal{B}_{ij,21} &= \mathcal{B}_{ij,12} = 0,
\end{aligned} \tag{13}$$

where $J_{\langle ij\rangle}$ is one if i and j are nearest neighbors, otherwise it is zero and $\delta_{i,j}$ is the Kronecker's delta. The stationary values, ϕ^s and ψ^s, are independent of the site label i. The last expressions in equation (13) were obtained considering ϕ_i and ψ_i equal to their stationary values, since we are interested in studying the equations satisfied by $\boldsymbol{\zeta}_i$ when the transients in the macroscopic equations (6) have died away.

The Langevin equation associated to the Fokker-Planck equation (12) is

$$\frac{\partial \boldsymbol{\zeta}_i}{\partial t} = \mathcal{A}_i\left(\boldsymbol{\zeta}_i\right) + \boldsymbol{\lambda}_i(t), \tag{14}$$

where

$$\langle \boldsymbol{\lambda}_i(t)\boldsymbol{\lambda}_j(t')\rangle = \mathcal{B}_{ij}\delta(t-t'). \tag{15}$$

Since $\mathcal{A}_i$ is linear in $\boldsymbol{\zeta}_i$, equation (14) can be solved in the Fourier space. Defining the Fourier transform, f_k, of a function f_j on a one dimensional network, with lattice spacing ℓ by:

$$\begin{aligned}
f_k &= \ell \sum_j \exp(-i\ell k j) f_j, \\
f_j &= \ell^{-1}\Omega^{-1}\sum_k \exp(-i\ell k j) f_k,
\end{aligned}$$

taking Fourier transforms in time and space of equation (15), and proceeding as in reference [21], we obtain

$$\langle \boldsymbol{\lambda}_k(\omega)\boldsymbol{\lambda}_{-k}(-\omega)\rangle = \mathcal{B}_k, \tag{16}$$

where ω and k stand for Fourier temporal frequencies and spatial wavelengths, respectively. For our model the explicit expressions for the elements of $\mathcal{B}_k$ are:

$$\begin{aligned}
\mathcal{B}_{k,11} &= \ell\Bigg(k_1 + r_1 k_1 \phi^s + k_2 \frac{\phi^s\psi^s}{1 + r_2\phi^s} \\
&\quad - 4\delta_1\phi^s(\cos(\ell k) - 1)\Bigg), \\
\mathcal{B}_{k,22} &= \ell\left(k_3 + r_3 k_3 \phi^s + k_4\psi^s - 4\delta_2\psi^s(\cos(\ell k) - 1)\right), \\
\mathcal{B}_{k,12} &= \mathcal{B}_{k,21} = 0.
\end{aligned} \tag{17}$$

Power spectra of the fluctuations close to equilibrium, $\langle|\xi_k(\omega)|^2\rangle$ and $\langle|\eta_k(\omega)|^2\rangle$, can be calculated by taking Fourier transform in time and space in the Langevin equation (14) and using equation (16). In particular, for our model they are given by:

see equations (18) *and* (19) *above.*

Stochastic pattern formation are generated when power spectra have a maximum at $\omega = 0$. From the power spectrum expressions, we can see that in the numerator the highest exponent for k is 6, while in the denominator the

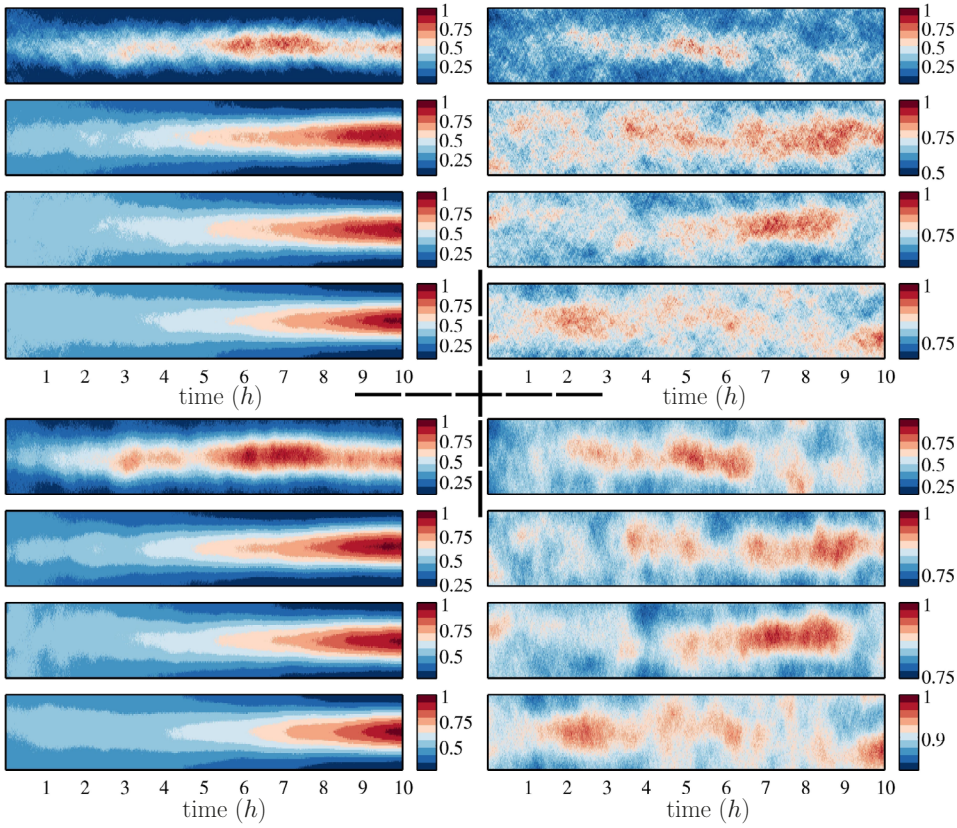

Fig. 2. Temporal evolution of **n**, (above), and **m**, (below) for different V values. From top to bottom V takes the values 1, 20, 40 and 100. Simulations were performed with the kinetic and diffusion parameters of Figure 1, with $\widehat{r}_2 = 0.16$ nM^{-1}. On the left panel $\widehat{r}_1 = 4$ nM^{-1} and Turing patterns are formed for all V. On the right panel $\widehat{r}_1 = 3.75$ nM^{-1}. For larger or smaller V quasi-patterns are spoiled. In this plot: y axis, membrane position; x axis, non scaled time; color scale, normalized **n** and **m** values.

highest exponent is 8. Thus, for k sufficiently large power spectra vanish. Then, the presence of a maximum is guaranteed if power spectra derivative with respect to k^2 are positive for small k. The phase diagram presented in Figure 1a shows that the region where power spectra have a maximum is larger than that for Turing patter formation, (black and gray areas).

Power spectra for $\widehat{r}_2 = 0.16$ nM^{-1} and selected $\widehat{r}_1$ values are shown in Figures 1b and 1c. Since all these selected $(\widehat{r}_2, \widehat{r}_1)$ pairs are in the gray zone of the phase diagram (Fig. 1a), we do not expect spatial order to arise, in terms of Turing pattern formation. However, power spectra have a peak that becomes more intense close to the boundary of the Turing region (black zone). For these parameters we expect to have quasi-pattern structures. However, if the intensity of the power spectra peak is not high enough, quasi-patterns would not be clearly formed.

5 Numerical results

In order to test our analytical results, we performed numerical simulations using the Gillespie Multi-Particle algorithm (GMP), which is equivalent to solving the master equation [29]. In order to apply the original Gillespie algorithm, we assumed that our system is well mixed. Thus, transfers of molecules between patches has to be greater than that for the reactions inside each patch. This condition is always hold for small ℓ, since the diffusion characteristic time, $\tau_D \propto \ell^2$, becomes much smaller than reaction characteristic times for sufficiently small ℓ. Simulations were performed with the same kinetic parameter values as those used in reference [8], unless we state otherwise. In order to correctly implement GMP algorithm, we calculated the transition rates using the reaction rate constants and the diffusion coefficients according to references [29,30]. However, in the text, we express the numerical values of the reaction rate constants for a more clear comparison with reference [8]. We considered a one dimensional grid with $\Omega = 50$ patches and different noise levels, which are related to the parameter V. If V is very small, just few particles are allowed to be in each patch leading to very strong internal fluctuations. However, if V increases, fluctuations become weaker and in the limit of V going to infinity the deterministic result should be recovered.

In Figure 2 we show the numerical results for **n**, (above), and **m**, (below). Simulation results are normalized to the final maximum value. The kinetic parameters of the left panel, are located at the black zone in

Figure 1a, i.e., Turing pattern formation conditions are fulfilled; while the right panel corresponds to the quasi-pattern region, (gray area). For each set of parameters four simulations with different V values are shown. Before performing the simulations we ran Gillespie algorithm in a grid of 50 patches, but without considering diffusion. We let the system evolve until its steady state which was used as an initial condition for the simulations with diffusion. Using this initial configuration, places where a stable maximum appears, are random. However, since we used periodic boundary conditions, we chose the central position for the maximum in order to have a nicer plot.

On the left panel of Figure 2 we show the temporal evolution of **n** and **m** for different V values. Turing patterns appear and remain very well formed along time. As we expected, for larger V the effects of finite sizes are mild and the system evolution has to be very close to the macroscopic solution. Pattern formation occurs even for small V, indicating that patterns are very robust appearing even for very strong noise levels, as it is the case for $V = 1$.

In the right panel of Figure 2, quasi-patterns are shown, in this case $\widehat{r}_1 = 3.75$ nM^{-1}. Quasi-patterns are not as sharp as Turing patterns. In general, the more intense the power spectrum peak, the more clear the quasi-patterns are. However, it also depends on the level of intrinsic noise. For large V, the system evolves to the macroscopic solution, which corresponds, for this set of parameters to a homogeneous state without Turing instabilities. Then, if V becomes large enough quasi-patterns are spoiled and their intensity reduces, (Fig. 2, $V = 100$). In addition, if V decreases and becomes very small, internal fluctuations are too intense that contribute negatively and quasi-patterns are also spoiled. In both cases, V large or small, quasi-patterns do not remain stable and they may be last few hours, (Fig. 2, $V = 1$ and $V = 40$). Although quasi-pattern simulation result for $V = 20$ are clearly different than those for Turing patterns, they last enough for the polarization process to occur.

The power spectra for the simulations shown in the right panel of Figure 2 are plotted in Figures 1b and 1c. In Figure 3 we show simulation results for lower power spectrum peak intensities, with $\widehat{r}_1 = 3.5$ nM^{-1}, (the two top panels), and $\widehat{r}_1 = 3.65$ nM^{-1} (the two lower panels) and $V = 20$. Since the power spectrum $\langle|\eta_k(\omega)|^2\rangle$ has a more intense peak than $\langle|\xi_k(\omega)|^2\rangle$, quasi-patterns in **m** are more clear than those in **n**. If the power spectrum peak intensity is not high enough quasi-patterns are not stable, vanishing in a short period of time and, some times, reappearing in a different membrane position (see the two top panels in Fig. 3).

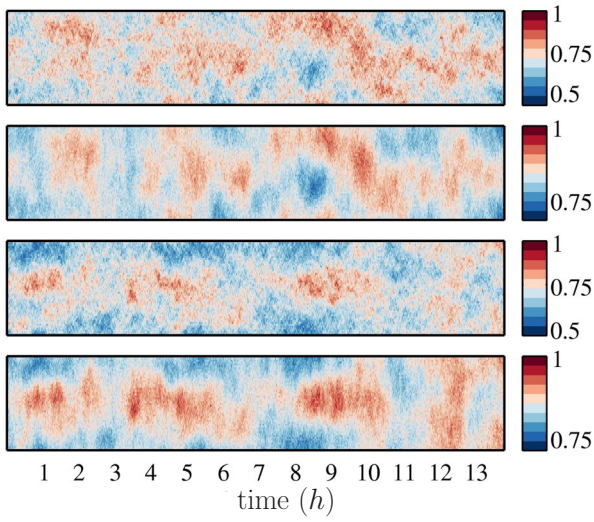

Fig. 3. Temporal evolution of quasi-patterns with less power spectra peak intensity. Simulations were performed with the kinetic and diffusion parameters of Figure 1, with $\widehat{r}_2 = 0.16$ nM^{-1} and $V = 20$. Temporal evolution of **n** (top panel), and **m** (second panel), for $\widehat{r}_1 = 3.5$ nM^{-1}. Simulations of **n** (third panel), and **m** (fourth panel), for $\widehat{r}_1 = 3.65$ nM^{-1}. In this plot: y axis, membrane position; x axis, non scaled time; color scale, normalized **n** and **m** values.

6 Conclusions

In this work we presented a stochastic model for describing neuronal polarization. This conceptual model was based on an activator-inhibitor model whose deterministic version was presented in reference [8].

The results presented here show that patterns are very robust, since they appear and remain stable even for high intrinsic noise levels, allowing cell to polarize with just few particles. We have also shown that intrinsic fluctuations can generate quasi-pattern structures. In general stochastic spatial patterns are not as sharp and robust as Turing patterns. Although in the presence of small noise, deterministic results should be obtained and the quasi-patterns vanish, when the level of noise increases quasi-patterns seem to be more stable and well defined. However, for too much noise, unstable quasi-patterns are obtained again. This would indicate that there is an optimal levell of noise for quasi-pattern formation.

Although quasi-patterns are different than Turing patterns, they can be very well defined for an interval of time of few hours, even for high or relatively low noise levels, (see Fig. 2, $V = 1$ and $V = 40$). Even in these cases cells could be able to polarize, since these localized concentration of molecules for such a period of time could increase active transport in the region and use it to sustain the quasi-pattern [31]. Quasi-pattern structures can be formed with less positive feedback strength than Turing patterns. Although power spectra have a maximum even for very low r_1 values, quasi-patterns formation depends on their peak intensity, which decreases for small r_1.

Turing patterns and quasi-patterns form structures that present a single pole with high active concentration of membrane proteins and modulator of endocytosis. Turing patterns are very well defined even in systems with high intrinsic noise and there are no restrictions in the number of molecules needed for their appearance. Although quasi-patterns sustainment depends on the number of molecules in the system, they can induce cell polarization by the

action of other mechanisms, such as active transport. Our work indicates that intrinsic noise would increase the chances for symmetry breaking, since in the presence of intrinsic noise cell polarization could occur even with less positive feedback strength.

S.A.M. thanks the hospitality of Prof. Enrico Carlon at the Institute for Theoretical Physics, KU Leuven, where this work was finished. This work was supported by Marie Curie Actions (FP7-PIIF-GA-RP-2012-991466), SeCyT-UNC (Project 3072011-0100436) and CONICET (Argentina). H.S.W. acknowledges financial support from MINECO (Spain), through Project PRI-AIBAR-2011-1323.

Appendix

In this Appendix we give some technical details for carrying out the system-size expansion of the master equation presented in this paper. We assume that the expansion parameter is V, i.e., each patch is treated as a subsystem whose volume becomes large. The system-size expansion [9,10] involves the change of variables, $\mathbf{n} = V\boldsymbol{\phi}(t) + V^{1/2}\boldsymbol{\xi}$ and $\mathbf{m} = V\boldsymbol{\psi}(t) + V^{1/2}\boldsymbol{\eta}$, as we have already defined in the main text. The vectors $\boldsymbol{\phi}(t)$ and $\boldsymbol{\psi}(t)$ are time-dependent vectors, and the vectors $\boldsymbol{\xi}$ and $\boldsymbol{\eta}$ stand for the stochastic contributions. The four of them have as many components as patches in the system. The way we proceed is equivalent to those presented in references [21,22].

The operators $\mathbb{E}_{n_i}^{\pm 1}$ and $\mathbb{E}_{m_i}^{\pm 1}$ that change n_i and m_i into $n_i \pm 1$ and $m_i \pm 1$, respectively; and therefore ξ_i into $\xi_i \pm V^{-1/2}$ and η_i into $\eta_i \pm V^{-1/2}$, are given by:

$$\mathbb{E}_{n_i}^{\pm 1} = 1 \pm V^{-1/2}\frac{\partial}{\partial \xi_i} + \frac{V^{-1}}{2}\frac{\partial^2}{\partial \xi_i^2} + \dots, \tag{A.1}$$

$$\mathbb{E}_{m_i}^{\pm 1} = 1 \pm V^{-1/2}\frac{\partial}{\partial \eta_i} + \frac{V^{-1}}{2}\frac{\partial^2}{\partial \eta_i^2} + \dots \tag{A.2}$$

Taking into account that the time derivative in equation (4) is taken considering constant $\mathbf{n}$ and $\mathbf{m}$, we have:

$$\frac{\partial P(\mathbf{n},\mathbf{m},t)}{\partial t} = \frac{\partial \Pi}{\partial t} - V^{1/2}\left(\nabla_{\boldsymbol{\xi}}\Pi\cdot\frac{d\boldsymbol{\phi}}{dt} + \nabla_{\boldsymbol{\eta}}\Pi\cdot\frac{d\boldsymbol{\psi}}{dt}\right), \tag{A.3}$$

where $\Pi(\boldsymbol{\xi},\boldsymbol{\eta},t) = P(\mathbf{n},\mathbf{m},t)$. We also have to consider that:

$$\begin{aligned} h\left(\frac{n_i}{V}\right) &= h\left(\phi_i + V^{-1/2}\xi_i\right) \\ &\approx h(\phi_i) + h'(\phi_i)V^{-1/2}\xi_i + \frac{h''(\phi_i)}{2}V^{-1}\xi_i^2 + \dots \end{aligned} \tag{A.4}$$

Inserting these last equations into equation (4) and considering equation (5), the master equation in the new variables takes the form:

$$\begin{aligned} &\frac{\partial \Pi}{\partial t} - \sqrt{V}\left(\nabla_{\boldsymbol{\xi}}\Pi\cdot\frac{d\boldsymbol{\phi}}{dt} + \nabla_{\boldsymbol{\eta}}\Pi\cdot\frac{d\boldsymbol{\psi}}{dt}\right) \\ &= \sum_{i=1}^{\Omega}\Bigg\{\left(-\frac{1}{\sqrt{V}}\frac{\partial}{\partial\xi_i} + \frac{V^{-1}}{2}\frac{\partial^2}{\partial\xi_i^2}\right) \\ &\times\left(Vk_1 + r_1k_1(V\phi_i + \sqrt{V}\xi_i)\right)\Pi \\ &+\left(\frac{1}{\sqrt{V}}\frac{\partial}{\partial\xi_i} + \frac{1}{2V}\frac{\partial^2}{\partial\xi_i^2}\right)k_2\left(h(\phi_i) + \frac{h'(\phi_i)}{\sqrt{V}}\xi_i\right) \\ &\times(V\phi_i + \sqrt{V}\xi_i)(V\psi_i + \sqrt{V}\eta_i)\Pi \\ &+\left(-\frac{1}{\sqrt{V}}\frac{\partial}{\partial\eta_i} + \frac{1}{2V}\frac{\partial^2}{\partial\eta_i^2}\right) \\ &\times\left(Vk_3 + r_3k_3(V\phi_i + \sqrt{V}\xi_i)\right)\Pi \\ &+\left(\frac{1}{\sqrt{V}}\frac{\partial}{\partial\eta_i} + \frac{1}{2V}\frac{\partial^2}{\partial\eta_i^2}\right)k_4(V\psi_i + \sqrt{V}\eta_i)\Pi \\ &+\sum_{j\leftrightarrow i}\Bigg[\left(\frac{1}{\sqrt{V}}\frac{\partial}{\partial\xi_i} - \frac{1}{\sqrt{V}}\frac{\partial}{\partial\xi_j} + \frac{1}{2V}\left(\frac{\partial}{\partial\xi_i} - \frac{\partial}{\partial\xi_j}\right)^2\right) \\ &\times\frac{\delta_1}{z}(V\phi_i + \sqrt{V}\xi_i)\Pi \\ &+\left(\frac{1}{\sqrt{V}}\frac{\partial}{\partial\xi_j} - \frac{1}{\sqrt{V}}\frac{\partial}{\partial\xi_i} + \frac{1}{2V}\left(\frac{\partial}{\partial\xi_i} - \frac{\partial}{\partial\xi_j}\right)^2\right) \\ &\times\frac{\delta_1}{z}(V\phi_j + \sqrt{V}\xi_j)\Pi \\ &+\left(\frac{1}{\sqrt{V}}\frac{\partial}{\partial\eta_i} - \frac{1}{\sqrt{V}}\frac{\partial}{\partial\eta_j} + \frac{1}{2V}\left(\frac{\partial}{\partial\eta_i} - \frac{\partial}{\partial\eta_j}\right)^2\right) \\ &\times\frac{\delta_2}{z}(V\psi_i + \sqrt{V}\eta_i)\Pi \\ &+\left(\frac{1}{\sqrt{V}}\frac{\partial}{\partial\eta_j} - \frac{1}{\sqrt{V}}\frac{\partial}{\partial\eta_i} + \frac{1}{2V}\left(\frac{\partial}{\partial\eta_i} - \frac{\partial}{\partial\eta_j}\right)^2\right) \\ &\times\frac{\delta_2}{z}(V\psi_j + \sqrt{V}\eta_j)\Pi\Bigg]\Bigg\}. \end{aligned} \tag{A.5}$$

The terms of order $\sqrt{V}$ in equation (A.5) yield the macroscopic equation (6), while keeping the terms proportional to V^0 we obtain the Fokker-Planck equation (12).

References

1. C.G. Dotti, C.A. Sullivan, G.A. Banker, J. Neurosci. **8**, 1454 (1988)
2. A. Caceres, B. Ye, C.G. Dotti, Curr. Opin. Cell Biol. **24**, 547 (2012)
3. S.J. Altschuler, S.B. Angenent, Y. Wang, L.F. Wu, Nature **454**, 886 (2008)
4. A.H. Chau, J.M. Walter, J. Gerardin, C. Tang, W.A. Lim, Cell **151**, 320 (2012)
5. A. Grupta, Ann. Appl. Probab. **22**, 827 (2012)
6. G.R. Walther, A.F.M. Marée, L. Edelstein-Keshet, V.A. Grieneisen, Bull. Math. Biol. **74**, 2570 (2012)

7. T. Freisinger, B. Klunder, J. Johnson, N. Muller, G. Pichler, G. Beck, M. Costanzo, C. Boone, R.A. Cerione, E. Frey, R. Wedlich-Soldner, Nat. Commun. **4**, 1807 (2013)
8. S.A. Menchón, A. Gärtner, P. Román, C.G. Dotti, PLoS ONE **6**, e24190 (2011)
9. N.G. van Kampen, *Stochastic Processes in Physics and Chemistry* (Elsevier, 2007)
10. H.S. Wio, R.R. Deza, J.M. López, *An Introduction to Stochastic Processes and Nonequilibrium Statistical Physics*, Revised edition (World Scientific, Singapore, 2012)
11. P. De Camilli, R. Jahn, Annu. Rev. Physiol. **52**, 625 (1990)
12. B.L. Tang, J. Neurochem. **79**, 923 (2001)
13. M.D. Onsum, C.V. Rao, Curr. Opin. Cell Biol. **21**, 74 (2009)
14. S. Mayor, R.E. Pagano, Nat. Rev. Mol. Cell Biol. **8**, 603 (2007)
15. G.J. Doherty, H.T. McMahon, Annu. Rev. Biochem. **78**, 857 (2009)
16. S. Etienne-Manneville, A. Hall, Nature **420**, 629 (2002)
17. S.D. Conner, S.L. Schmid, Nature **422**, 37 (2003)
18. K.R. Sanft, D.T. Gillespie, L.R. Petzold, IET Syst. Biol. **5**, 58 (2011)
19. A.J. McKane, T.J. Newman, Phys. Rev. E **70**, 041902 (2004)
20. J. Realpe-Gomez, T. Galla, A.J. McKane, Phys. Rev. E **86**, 011137 (2012)
21. C.A. Lugo, A.J. McKane, Phys. Rev. E **78**, 051911 (2008)
22. T. Biancalani, D. Fanelli, F. Di Patti, Phys. Rev. E **81**, 046215 (2010)
23. M.S. de La Lama, I.G. Szendro, J.R. Iglesias, H.S. Wio, Eur. Phys. J. B **51**, 435 (2006)
24. H. Wang, Z. Fu, X. Xu, Q. Ouyang, J. Phys. Chem. A **111**, 1265 (2007)
25. J.D. Murray, *Mathematical biology II: Spatial models and biomedical applications* (Springer, 2003)
26. M. Postma, L. Bosgraaf, H.M. Loovers, P.J.M. Van Haastert, EMBO Rep. **5**, 35 (2004)
27. Y. Sako, A. Nagafuchi, S. Tsukita, M. Takeichi, A. Kusumi, J. Cell Biol. **140**, 1227 (1998)
28. O. Thoumine, M. Lambert, R.-M. Mége, D. Choquet, Mol. Biol. Cell. **17**, 862 (2006)
29. D.T. Gillespie, J. Comput. Phys. **22**, 403 (1976)
30. F. Baras, M.M. Mansour, Phys. Rev. E. **54**, 411 (1996)
31. E. Marco, R. Wedlich-Soldner, R. Li, S.J. Altschuler, L.F. Wu, Cell **129**, 6139 (2007)